Submitted to the Astrophysical Journal
Preprint typeset using LATEX style emulateapj v. 14/09/00

EXPERIMENT DESIGN AND FIRST SEASON OBSERVATIONS WITH THE DEGREE ANGULAR SCALE INTERFEROMETER

E. M. Leitch, C. Pryke, N. W. Halverson, J. Kovac, G. Davidson, S. LaRoque, E. Schartman[1], J. Yamasaki, J. E. Carlstrom
University of Chicago, 5640 South Ellis Ave., Chicago, IL 60637
W. L. Holzapfel
University of California, 426 Le Conte Hall, Berkeley, CA 94720
M. Dragovan
Jet Propulsion Laboratory, California Institute of Technology, 4800 Oak Grove Drive, Pasadena, CA 91109
J. K. Cartwright, B. S. Mason, S. Padin, T. J. Pearson, M. C. Shepherd, A. C. S. Readhead
California Institute of Technology, 1200 East California Boulevard, Pasadena, CA 91125
Submitted to the Astrophysical Journal

ABSTRACT

We describe the instrumentation, experiment design and data reduction for the first season of observations with the Degree Angular Scale Interferometer (DASI), a compact microwave interferometer designed to measure anisotropy in the Cosmic Microwave Background (CMB) on degree and sub-degree scales (l = 100–900). The telescope was deployed at the Amundsen-Scott South Pole research station during the 1999–2000 austral summer and conducted observations of the CMB throughout the following austral winter. In its first season of observations, DASI has mapped CMB fluctuations in 32 fields, each 3°.4 across, with high sensitivity.

Subject headings: cosmology: cosmic microwave background—cosmology: observations —techniques:interferometric

1. INTRODUCTION

The use of the CMB angular power spectrum to constrain cosmological parameters has been the subject of much recent literature (see e.g., Hu & White (1996) for a discussion of salient features of the power spectrum). We are at a point where the ability to resolve fine-scale structure in the power spectrum is no longer limited primarily by detector sensitivity, but by experiment design, understanding of calibration uncertainties and careful control of systematics. The comparison of complementary measurements by experiments of radically different design will prove critical to an understanding of what exactly the CMB is telling us.

Because they directly measure Fourier components of the sky, interferometers are uniquely suited to measurement of the CMB power spectrum, and offer a completely independent technique, free of many of the systematics which need to be carefully controlled in scanning experiments. The Degree Angular Scale Interferometer (DASI), along with its companion instrument the CBI (Pearson 2000), and the VSA (Jones 1997), is one of a new generation of ultra-compact microwave interferometers designed to measure anisotropy in the CMB. With 13 elements operating in 10 1-GHz bands from 26–36 GHz, DASI provides dense sampling of the power spectrum from $l = 100$ to $l = 900$, angular scales spanning the first three harmonically related acoustic peaks in $\Omega \sim 1$ cosmologies.

This paper describes details of the instrument, design of the experiment, and calibration and reduction of the Fourier plane visibility data. Analysis of these data and extraction of the angular power spectrum are presented in Halverson et al. (2001), (hereafter Paper II), while limits on cosmological parameters from the DASI data are given in Pryke et al. (2001), (hereafter Paper III).

In sections §2 and §3 of this paper, we discuss details of the instrument design. A description of the site is given in §4. We describe the CMB observations in §5 and §6. Data reduction and analysis are presented in §7 and §8, and results are presented in §9.

2. INSTRUMENT

2.1. *Telescope Mount*

The telescope is situated atop the inner of two concentric towers attached to the Martin A. Pomerantz Observatory (MAPO), 0.7 km from the geographic South Pole. The inner tower is mechanically isolated from the outer tower to minimize vibrations transmitted from the building to the telescope. Although diurnal variations in the ambient temperature at the Pole are extremely small (see §4), the external legs of the inner tower are insulated to minimize tilt of the azimuth ring from differential thermal expansion by direct solar heating during the summer months.

A room beneath the telescope, attached to the outer tower, houses helium compressors, drive amplifiers, and an air handling unit for managing waste heat from the telescope and compressors. The interior of the telescope opens directly onto the compressor room, providing access to drive systems, receivers and electronics even in mid-winter, when the darkness and extreme cold (as low as −80 deg C ambient) severely restrict outside activity. An insulated fabric bellows permits motion in the elevation axis while maintaining the interior of the telescope and drive assemblies at room temperature using only waste heat from telescope control and correlator electronics. Tested for flexi-

[1] Currently at Princeton University

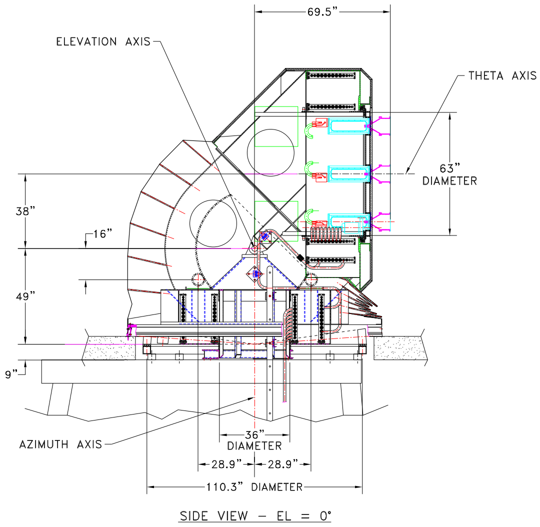

FIG. 1.— Schematic of the DASI telescope. Shown is a side view of the instrument, at EL = 0, with the faceplate pointing to the right.

bility to −100 deg C, the bellows has thus far functioned perfectly at polar temperatures.

The telescope mount is an altitude-azimuth design, employing a counterbalanced gear and pinion elevation drive, for tracking and pointing stability. Heavy box steel construction lends the mount extreme rigidity and immunity to flexure; the combined weight of the azimuth ring, elevation cradle and counterweights is approximately 35,000 lbs.

The absolute pointing of the telescope is derived from observations of bright stars made with a small optical camera mounted on the faceplate. In the automated pointing observation procedure, approximately 80 positions for stars distributed throughout the sky are acquired using a frame grabber. These observations are fit with an eight parameter pointing model, yielding $20''$ rms residuals. Limits on deviation of the radio pointing from this model are discussed in §8.

2.2. *Faceplate*

The interferometer has 13 primary antenna elements, arranged in a three-fold symmetric pattern on a rigid faceplate attached to the elevation cradle. The locations of the antennas in the faceplate were numerically optimized to provide nearly uniform sampling over the multipole range probed by DASI, $l \sim 100$–900 (see Figure 2). The rigid faceplate greatly simplifies the design of the correlator, since unlike conventional tracking arrays, projected baseline lengths for a co-planar array are independent of the pointing center, and tracking delays are not required.

The faceplate can also be rotated about its axis. In combination with the three-fold symmetry, this feature provides important diagnostic capabilities, for instance permitting discrimination of spurious signals due to cross-talk between the antenna elements. Since the antenna pattern repeats with every 120 deg of rotation, any signal in the far field remains unchanged by the rotation; signals due to cross-talk, however, will rotate with the faceplate. Moreover, at the South Pole, celestial sources track at fixed elevation, and the ability to simulate parallactic angle rotation provides a powerful consistency check for observations of calibrator sources, as described in §6.2. For purposes of imaging, the rotation also allows dense sampling of the Fourier plane (see §3).

2.3. *Primary Antenna Elements*

Each antenna consists of a 20-cm aperture, 30 deg semi-flare angle lensed corrugated horn, to achieve a diffraction limited beam on the sky. To make the array maximally compact, the receiver dewars were designed to fit entirely within the footprint of the horns; the shortest baseline is 25.1 cm. Unlike Cassegrain elements, horns provide unobstructed apertures, with lower sidelobe response and better cross-talk characteristics, important for a compact array in which the elements are nearly touching. Each antenna element is further surrounded by a corrugated shroud, yielding a measured monochromatic crosstalk level of less than −100 dB in laboratory measurements of the horn-lens combination (Halverson & Carlstrom 2001). To further suppress cross-talk from correlated amplifier noise, the receivers are also equipped with front-end isolators.

Each element is preceded by a high density polyethylene lens, resulting in a high aperture efficiency, 83.5%, and permitting an extremely compact horn design. At polar temperatures, the lens contributes less than 2.5 K to the system temperature.

The beam pattern, which determines the field of view of the interferometer, has been characterized in range measurements at 26, 30, and 36 GHz and in each case found to agree closely with the predicted pattern, both in the sidelobe response, which is typically −20 dB at the first sidelobe, and in the main beam width, which is $3\overset{\circ}{.}4$ FWHM at 30 GHz (Halverson & Carlstrom 2001). From the agreement between these measurements and the theoretical beam pattern, we adopt the theoretical value as our estimate of the true aperture efficiency and assign a

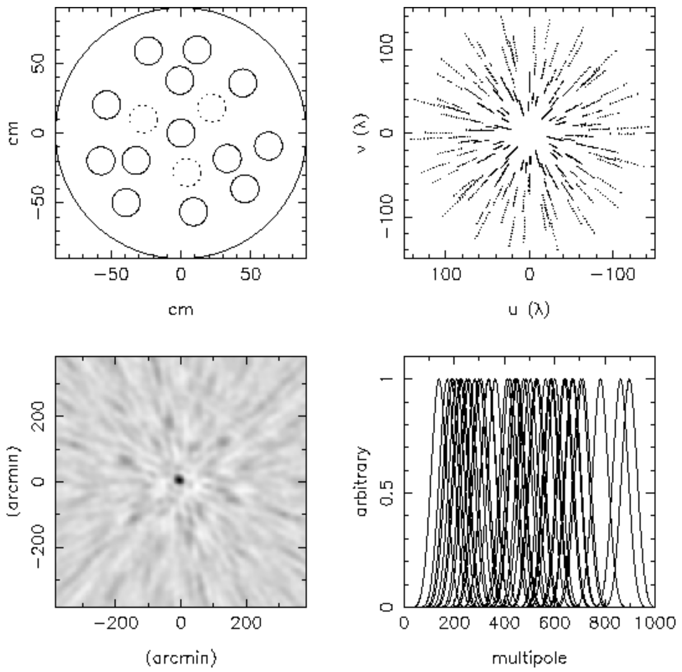

FIG. 2.— Top left: The DASI faceplate configuration. Closed circles represent locations of the 13 antennas. (Open circles are additional faceplate slots). Top right: The resulting instantaneous Fourier plane coverage of the interferometer, showing radial extension due to the frequency dependence of the (u, v) coordinates. Bottom left: one of the brightest point sources in the DASI fields, showing the synthesized beam pattern. Radial features in the image are artifacts of the sampling. Bottom right: The effective l-space window functions of the 26 distinct DASI baselines, shown for 26.5 and 35.5 GHz. Note that this represents only 1/5 of DASI's instantaneous l-space sampling.

fractional uncertainty of 4%, as shown in Table 1.

2.4. *Signal Chain*

Each receiver employs a cryogenically cooled, 4-stage InP HEMT amplifier operating from 26–36 GHz. These amplifiers were constructed at the University of Chicago, after a design developed at NRAO (Pospiezalski et al. 1995). Receiver temperatures range from 15–26 K at the center of the band, increasing to an average of 30 K at the band edges. These temperatures include the HEMT's, isolator and polarizer (all at 10 K), and warm throat, horn and lens. Including CMB and atmosphere, we achieve typical system temperatures of 26 K at band center, for an rms sensitivity per visibility of approximately 84 Jy $s^{1/2}$ in a 1 GHz band.

The 26–36 GHz RF signal from each antenna is mixed down to 2–12 GHz IF band using a local oscillator (LO) tuned to 38 GHz. The IF signal is split into 10 1-GHz wide bands, each of which is further mixed down to 1–2 GHz. The 13 signals at each frequency are fed to one of 10 identical analog correlators (Padin et al. 2000), where the 78 complex multiplications are formed, digitized and integrated for 0.84 s in a digital accumulator. A copy of each input signal is phase-shifted by 90 deg, and multiplications are performed simultaneously for the real and imaginary Fourier components. A 180 deg phase switch is applied to each LO in a Walsh sequence on a 25.6 μs clock interval and is demodulated by the accumulators, to remove any offsets or slowly varying pickup. To further reduce residual offsets, a second, slower level of 180 deg Walsh switching is applied to the LOs, and is demodulated in post-detection software with a switching period equal to the readout interval. The multiplier gains and quadrature errors are periodically calibrated by injection of a correlated broadband noise source at the input to each receiver.

Each analog correlator is integrated onto a single full-depth VME card, and the entire 10 GHz correlator fits into a crate approximately 75 cm on a side. Filtering and down-conversion of the IF signal is accomplished in a similar crate, and both rotate with the antennas on the underside of the telescope faceplate. The short fixed distance from the receivers to the downconverter and correlator eliminates flexure of cables carrying phase-sensitive signals, resulting in excellent phase stability; observed instrumental phase drifts are less than 10 deg over a period of many weeks.

3. INTERFEROMETER CHARACTERISTICS

An interferometer directly measures components of the Fourier transform of the sky brightness. The response on the sky for a two-element interferometer is a sinusoidal interference fringe pattern, oriented perpendicular to the baseline vector **B** connecting the two elements. The spacing of the fringe pattern is λ/B, where λ is the observing wavelength and B is the magnitude of the projection of **B** perpendicular to the line of sight. Each baseline of a multi-element array therefore probes a point in Fourier space given by $(u, v) = (B_x/\lambda, B_y/\lambda)$, or in terms of multipole moment, $l \simeq 2\pi B/\lambda$ (for $l \gtrsim 60$) (White et al. 1999); shorter baselines measure larger angular scales, and vice versa.

The fringe pattern on the sky is enveloped by the primary beam of the array elements. The output of the interferometer, the *visibility*, is the time-averaged integral of this pattern, multiplied by the sky brightness (see Paper II for a rigorous definition), and is the fundamental data quantity discussed in these papers.

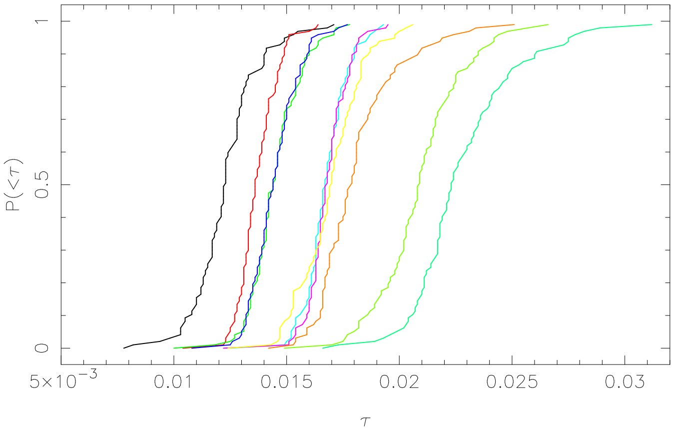

FIG. 3.— Cumulative opacity distributions, by frequency, at the South Pole, from 05 May–07 November 2000. The ten curves in this plot, from left to right, are for frequencies from 26.5 to 35.5 GHz in 1 GHz steps.

With 13 elements, the DASI array yields 78 distinct baseline vectors; the frequency dependence of the (u, v) coordinates means that with 10 frequency channels, DASI samples 780 different points in the Fourier plane, although visibilities from neighboring frequencies of the same baseline are highly correlated (see Figure 2). The 3-fold symmetry of the faceplate reduces the number of unique baseline lengths to 26, each pointing of the telescope producing 3 independent measurements of the same multipole at each frequency. With baseline separations ranging from 25.1–120.7 cm, DASI samples multipole moments from $l = 140$ at the lowest frequency to $l = 900$ at the highest.

Images of the sky can be produced from an interferometer by simple Fourier inversion of the visibilities. The transform of the (u, v) sampling defines the effective resolution of the image, the so-called *synthesized beam*; for DASI, the instantaneous (u, v) coverage produces a synthesized beam width of approximately $20'$ (FWHM), with radial sidelobes due to the radial frequency structure of the (u, v) sampling (top right of Figure 2).

Rotation of the faceplate preserves the baseline lengths, but rotates the fringe pattern on the sky. This feature can be used to obtain additional independent samples of the same multipole moment in a given field, or for purposes of imaging, to reduce sampling artifacts in the synthesized beam by filling in the (u, v) plane. With the 3-fold redundancy, the pattern of (u, v) coverage repeats with each 60 deg of rotation, allowing the same Fourier component to be measured by independent baselines.

TABLE 1
SUMMARY OF ARRAY PARAMETERS

Primary antenna elements	13
Aperture Diameter	20 cm
Beamwidth (30 GHz)	$3\overset{\circ}{.}4 \pm 0\overset{\circ}{.}07$
Aperture Efficiency	0.835 ± 0.033
Gain	9.5 ± 0.4 μK/Jy
Band	$26 - 36$ GHz
Correlator IFs	10×1 GHz
Rms Sensitivity (1 GHz band)	~ 84 Jy s$^{1/2}$
$B_{\rm min}$	25.1 cm
$B_{\rm max}$	120.73 cm

4. THE SOUTH POLE ENVIRONMENT

Located high on the Antarctic plateau, at an altitude of 2.8 km, the South Pole station offers a unique astronomical environment, ideal for CMB observations, where long integration times are required to detect signals millions of times weaker than the typical system temperature of a HEMT-amplified receiver. Situated less than a kilometer from the geographic South Pole, DASI can track fields continuously, with no variation in airmass. Sunrise and sunset at the Pole occur once per annum, at the equinoxes; for six months of the year the sun is below the horizon. Rising and setting of the moon occur once every month, yielding two weeks per month of continuous dark time. (Naturally, these sources never rise higher than $\sim 23\overset{\circ}{.}5$ above the horizon.) The slow variation in astronomical conditions at the Pole contributes to the extreme stability of the local environment; the peak-to-peak diurnal temperature change, averaged over 1999–2001, is less than 6 degC.

The Antarctic plateau is one of the driest deserts on the planet, with annual precipitation averaging less than 8 g/cm^2. Moreover, cooling over the poles flattens the troposphere, so that the polar atmosphere has a lower water column density than other sites of the same physical altitude; radiosonde measurements above the Pole indicate that the tropopause occurs between 8 and 9 km, compared to 11–13 km nearer the equator. The precipitable water vapor column above the pole varies between 0.25 and 0.7 mm annually (Chamberlin & Bally 1995). The polar airmass is also very stable, with surface winds dominated by a weak katabatic flow from gently sloping higher terrain several hundred kilometers away (see discussion in King & Turner 1997). Measured fluctuations in atmospheric emissivity at microwave frequencies are minimal, making the South Pole a premier site for degree scale imaging of the CMB (Lay & Halverson 2000). Our data confirm the superiority of the site—less than 5% of the data from the first season of observations is rejected due to weather (see §7).

Opacities were measured with DASI from skydips performed daily during May–November 2000. The mean opacity determined from these data rises from $\tau = 0.012$ to $\tau = 0.023$ over the DASI frequency band (26–36 GHz), with little day-to-day variation; at the lowest frequency, 95% of the measured opacities are < 0.015, while at the highest frequency, 95% are < 0.028 (see Fig 3). At typical ambient temperatures during the winter (-60 deg C) these results indicate that over much of the DASI band, the CMB and the atmosphere contribute roughly equal amounts to our system temperatures.

5. DESIGN OF THE EXPERIMENT

5.1. *Field Selection*

The DASI experiment is designed to avoid known foreground contaminants; although DASI's frequency band was selected in part for the availability of low-noise amplifiers in the 26–36 GHz range, the CMB is expected to dominate over Galactic synchrotron and free-free emission at frequencies above 20 GHz (Tegmark et al. 2000).

Thermal emission from dust should be insignificant for experiments below 100 GHz. However, recent observations suggest that non-thermal emission associated with the dust may contaminate small-scale anisotropy measurements at a level comparable to the CMB in the $l \sim 600$ range (Leitch et al. 1997), at least at frequencies below 30 GHz. This emission has been attributed to dipole radiation from spinning dust grains aligned with the local magnetic field (Draine & Lazarian 1998). Fortunately, the South Pole provides access to a large region of sky with some of the lowest overall dust column densities, and field positions are chosen to coincide with the minimum in the IRAS 100 micron map of the southern sky (see Figure 4).

Four rows of eight fields, referred to as the A–D rows, were arranged on a hexagonal grid (to facilitate eventual mosaicing of the fields), spaced by 1 h in RA and 6 deg in declination. The grid of fields was positioned at high elevation (≥ 49 deg), to minimize contamination from the ground. The spacing of 1 h in RA permits a constraint on ground contamination, as discussed below, while at the same time minimizing inter-field correlations, greatly simplifying the analysis described in Paper II. Declinations and right ascensions of the easternmost field in each row are given in Table 2.

Little is known about the distribution of point sources at high frequencies, and at best, fields can be selected only to avoid bright sources from low frequency catalogs. Moreover, placing fields on a regular grid further restricts our ability to avoid even known point sources. Methods for dealing with point source contamination are described in §8, and in Paper II.

TABLE 2
CMB Field Row Positions[a]

Row	RA (J2000)	Dec (J2000)	Days Observed
A	21 59 58.93	−60 59 44.0	14
B	21 30 01.86	−66 59 39.6	24
C	22 30 02.34	−54 59 40.7	28
D	23 00 03.03	−48 59 47.8	31

[a] Field positions are obtained by adding 0–8 h to the RA listed for each row.

5.2. *Ground Contamination*

Astronomical foregrounds aside, the presence of ground contamination at a level much greater than the expected cosmological signal places the most stringent constraint on our observing strategy. Although DASI was intended to operate with a ground shield, the panels could not be installed until the 2000–2001 austral summer and were not in place while the data described here were collected.

The signature of the ground is visible even in short integrations; as fields are tracked over the full azimuth range, excluding the MAPO building, variations as large as $7\,\sigma$ above the expected thermal noise ($\sim$ 5 Jy) can be seen in 5-minute integrations, while directly over the roof of MAPO, $20\,\sigma$ signals are seen on a few of the shortest baselines. However, these fluctuations are strongly dependent on baseline length, falling sharply with increasing (u, v) radius; on the longest baselines, the raw visibilities are consistent with thermal noise at all frequencies, even when observing directly over the MAPO building.

Although the ground shows a strong azimuthal dependence, repeated 24 hr tracks demonstrate that the signals are quite stable in time. When data taken as much as five days apart are differenced, the residuals are consistent with the thermal noise, even on the shortest baselines, and over the full azimuth range, including directions towards MAPO and other station buildings.

Because the ground signal exhibits long-term stability, our strategy was to observe independent fields over a narrow azimuth range on timescales short enough that the ground could be expected to remain constant. Observations were divided among groups of 8 fields separated by 1 h of RA, each group at a constant elevation. Each field in a group was observed over a fixed 1 hr azimuth range; over the course of 8 hours, these observations yield 8 samples of the CMB sky, and 8 independent samples of the same ground, allowing a constraint on the common mode (and reducing the effective number of degrees of freedom available for constraining the CMB power spectrum). Observations were timed so that data from each field sampled precisely the same ground. Azimuth ranges were selected which avoided lines of sight passing over any of the South Pole station or science buildings, or the communications antenna field.

5.3. *Observing Schedule*

As described above, in each 24 hr period, we obtained a total of 16 hours of integration on 8 CMB fields, 8 hours over each of two azimuth ranges. The remainder of a 24 hr period was divided among various calibration tasks. Every 8 hr period was bracketed by 1.5 hr scans on a calibrator source, as discussed in the next section, and these 11 hr periods were in turn bracketed by skydips, yielding 2 independent measures of the atmospheric opacity daily. These data are described in §4. Finally, at the beginning and end of every 24 hr period, the noise source was used to calibrate the complex correlator, as described in the next section.

6. CALIBRATION

Several kinds of calibrations are performed for each of DASI's 78 baselines, in each of the 10 bands: 1) calibration of the complex multipliers to correct for non-orthonormality of the real and imaginary visibility response, 2) absolute calibration of the flux scale for each baseline, which is transferred to a celestial source, and 3) regular observations of celestial calibrators, to refer visibility amplitudes to the absolute flux scale and visibility

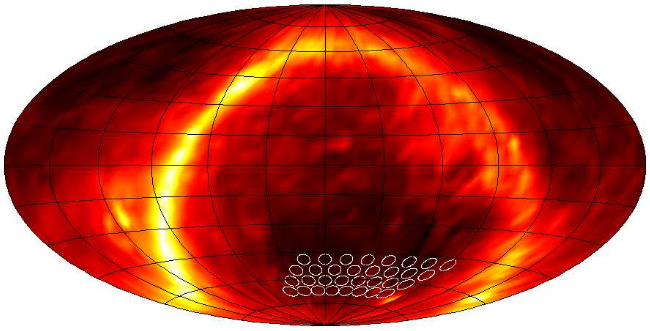

FIG. 4.— Locations of the DASI CMB fields, plotted over the IRAS 100 micron map, in celestial coordinates. (Color map is logarithmic, spanning 4 decades of intensity.)

phases to a phase center.

The second and third of these calibration tasks are described in separate sections below. The first, the calibration of the complex multipliers, was accomplished by injection of a strong signal from the correlated noise source. This calibration was performed at the beginning and end of every 24 hr period, although for 95% of all baselines, the rms variation of the relative gain and phase offset between real and imaginary multipliers were less than 2% and 1°.2, respectively, over 97 days.

6.1. *Absolute Calibration*

The relative scarcity of sources whose fluxes are known at high frequencies makes absolute calibration of any microwave experiment a challenging proposition, as does the generic steepness of most radio source spectra. Additionally, of the sources which are well studied, few are accessible from the South Pole. Planets never rise more than $\sim 23°.5$ above the horizon, and the best studied of these, Jupiter and Mars, were either very low or below the horizon throughout the 2000 observing season. Moreover, with DASI's 20-cm apertures, beam dilution makes it inherently difficult to detect all but the brightest point sources; with a gain of approximately 10 μK/Jy, to achieve a S/N ~ 1 on a 1 Jy source requires about 3 hours of observation.

Consequently, the absolute calibration of DASI is based on measurements of beam-filling external thermal loads of measured temperature. The noise source power level (which is separately monitored for drift) was calibrated for each receiver from these measurements, and a calibration of correlated noise source power was derived for each baseline. This calibration was immediately transferred from the noise source to a celestial source.

For the transfer observations, the source was tracked for 3 hours at each of six faceplate rotations, separated by 60 deg, with a reference field observed for ground subtraction. Due to the three-fold symmetry of the antenna locations, this procedure yielded six independent measurements of each (u, v) point from different baselines with different contributions from the ground. The source model was averaged over these observations to reduce any residual systematics, resulting in a determination of the flux for each baseline with a statistical uncertainty of $< 2\%$.

The load measurement and transfer procedure was conducted once during the austral summer of 2000 and again in the summer of 2001. The calibration of 2001, on which the absolute scale of the DASI observations is based, was transferred directly to PKS J0859-4731. The 2000 calibration was transferred without ground subtraction to the Carina nebula, and later to PKS J0859-4731 through interlaced observations of the two sources. We estimate the statistical uncertainty on the overall flux scale resulting from the load measurement procedure and transfer observations to be $< 1\%$, averaged over baselines. Consistent with this estimate, the average ratio of fluxes derived from the independent calibrations of 2001 and 2000 is 0.997. The systematic uncertainty common to these two calibrations, resulting mainly from uncertainty in the determination of antenna coupling to the loads and in the effective load temperatures, we estimate to be 3%, and is the dominant contribution to the total 3.5% uncertainty in the overall flux scale.

6.2. *Celestial Calibrators*

As previously noted, each 8 hr period of CMB observations was bracketed by 1.5 hr scans of celestial calibrators, to refer the visibility amplitudes to the absolute flux scale and to refer the phases to a common phase center. In addition, the correlated noise source was injected every hour, to track short-term system stability. In practice, the instrumental phase and amplitude response were quite stable; over 97 days of observation, the phases showed a typical rms variation of less than 15 deg.

For the fields referred to as the A-row in Table 2, the amplitude calibrator used was the Carina nebula, a well-known Galactic HII complex. The Carina nebula's free-free spectrum makes it a good high frequency calibrator; the source is bright enough that its flux can be measured to a few percent on most baselines in approximately 15 minutes. However, the source is dominated by an extended central region, with much weaker flux on smaller scales, necessitating significantly longer integrations on the longest baselines to achieve uniform accuracy.

These considerations led us to use PKS J0859-4731, a more compact Galactic HII region, as the flux calibrator for the B–D row observations. Although its integrated flux is lower than that of the Carina nebula (see Leitch (2000)), the source is readily detectable, with nearly uniform brightness ($\sim$ 150 Jy) out to the longest baselines; for (u, v) radii $> 80\ \lambda$, the source is considerably brighter than Carina.

Although PKS J0859-4731 is partially resolved by the longest baselines, observations of the source while rotating the faceplate show that the mean phase variation with parallactic angle over all baselines is less than 10 deg rms. These observations indicate that PKS J0859-4731 is sufficiently point-like (or at least radially symmetric) that the source can be used as a phase calibrator. Although PKS J0859-4731 is located in the Galactic plane, these observations require any contaminating flux from the Galaxy to be nearly uniform.

Thus, for the B–D row data, each 1.5 hr scan was spent observing PKS J0859-4731, which was used as both amplitude and phase calibrator. For the A-row observations, this time was split between the Carina nebula and the extragalactic source Centaurus A, which was used as the phase calibrator. On all but the longest baselines of the A-row data, these observations yielded measurements of both phase and amplitude to better than 2%.

7. DATA REDUCTION

The data presented in this paper (and in Papers II and III), comprise 97 days of observations obtained during 05 May–07 November 2000, divided among 32 fields, as described in §5.1. These data represent an observing efficiency of approximately 85%, of the time devoted exclusively to CMB observations; the remainder were lost to abnormal aborts of an observing run due to timing or tracking errors, or to hardware maintenance. Because our ability to constrain the ground depends critically on uniform sampling of a fixed azimuth range for each of 8 fields, as described in §5.2, a draconian pre-edit is applied to the CMB data – the complete loss of data for any single field for any reason results in the rejection of an entire 8 hours of data.

Visibilities are accumulated from each correlator in 8.4 s integrations, along with monitor data from the telescope drive systems and receivers. Prior to combination for input to the power spectrum analysis described in Paper II, various edits are applied to these data, falling into three general categories: cuts on monitor data, cuts derived from the visibility data themselves, and calibration edits.

In the first category, data are rejected when a receiver is not operating, when a receiver LO loses lock, or when either the 10 or 50 K cryogenic receiver stages shows a gross warming trend; these cuts typically reject $\sim 5\%$ of the data. Next, data are edited on the quadrature errors in the complex multipliers, determined twice daily by injection of a broad-band noise source. Baselines for which the relative gain between the real and imaginary multipliers falls outside the range 0.9 ± 0.3, or for which the phase offset falls outside the range $0\,\mathrm{deg} \pm 20\,\mathrm{deg}$ are rejected. These ranges are determined from the empirical distribution of quadrature errors, and reflect the values at which the distributions become significantly non-Gaussian; these data are interpreted as evidence for microstrip termination errors, or malfunctioning multiplier chips. When the raw visibilities are calibrated for these offsets, data are rejected if the bracketing values differ by more than 10%. Cuts on the quadrature errors collectively reject $\sim 11\%$ of the data.

Scans on the CMB fields are then trimmed so that the data remaining after the edits described above sample the same azimuth range for each field, typically rejecting a further 9%. The closest approach of the moon to the DASI fields during their observation is 40°. Fringing from the moon is evident on the shortest baselines, and for (u,v) radii $< 40\,\lambda$, we reject all data when the moon is above the horizon. The D-row data observations were made from 11 September–11 October, bracketing the sunrise, with an additional week obtained in early November; data for the D-row fields are also excluded for (u,v) radii $< 40\,\lambda$ when the sun is above the horizon.

In the second category of edits, the raw visibilities are combined into 1 hr bins, and the baseline-baseline correlation matrix is computed separately for each correlator. Large off-diagonal elements of the correlation are interpreted as evidence for contamination by atmospheric fluctuations. By comparison of data for the same field from different azimuth ranges on the same day, or from different days, we find that the precise threshold of the correlation cut does not strongly affect data consistency, and we reject an 8 hr observation for which any off-diagonal element exceeds ± 0.36, affecting 5% of the data.

In the last category, data are edited on the quality of the associated observations of celestial phase and amplitude calibrators. Data are rejected when the bracketing calibrator amplitudes vary by $> 5\%$, or when the bracketing phases change by > 30 deg. Data are also rejected when previous edits have reduced the sensitivity on a calibrator scan by $> \sqrt{2}$, resulting in a statistical error of $> 3\%$. On average, these cuts reject $\sim 20\%$ of the data. Overall, the combined edits from all categories reject a total of 40% of the data.

For input to the power spectrum analysis described in Paper II, the edited and calibrated data are combined into 1 hr integrations, yielding a maximum of 1560 visibilities per field (78 complex baselines$\times$10 correlator channels) for each observation.

8. POINT SOURCES

As expected for high-frequency, small angular scale experiments, point sources are the dominant astronomical foreground for DASI (see e.g., Tegmark & Efstathiou (1996)). The brightest point sources in our fields are obvious in the synthesized maps (see Figure 2), even without ground subtraction. However, as discussed in Paper II, to extract the CMB power spectrum from the visibility data, we employ a constraint matrix method, capable of projecting out foregrounds on the basis of their spatial template alone. To null the effect of point sources through this technique we therefore require only the positions of the sources, *not their fluxes*.

As discussed in Paper II, we construct the list of point sources to null using a combination of source positions derived from the DASI data, as well as positions of sources in the PMN southern catalog (Wright et al. 1994). Here, we describe the procedure used to find sources in the DASI data.

For each set of fields, images are made from ground-subtracted visibilities, using the DIFMAP imaging package (Shepherd, Pearson, & Taylor 1994). When making the images, baselines $< 64\ \lambda$ are excluded; this cut removes the bulk of the CMB power in the data, significantly increasing S/N for point source detection. The maps are then divided into annular bins around the field center; the pixel rms in each bin, averaged over 8 fields, is fit to a noise model, consisting of a CMB signal multiplied by the primary beam, added to a flat detector noise floor (as in

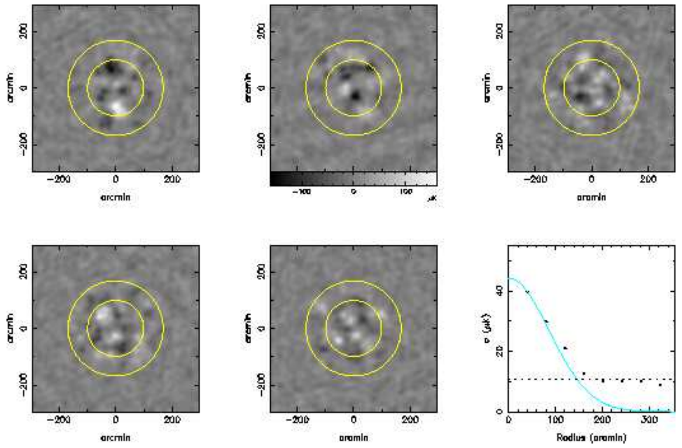

FIG. 5.— Images of five DASI CMB fields. The two concentric circles represent the −3 dB and −10 dB taper of the beam, respectively. The lower right panel shows the rms pixel values for field 5 (lower middle panel) as a function of radius (black points), the primary beam taper normalized to the first rms pixel value (solid line), and the theoretical rms image noise, determined from the scatter in 8.4 s visibility data (dashed line).

the bottom right panel of Figure 5). Each image is then divided by the fitted noise model to produce an effective S/N map. The highest peaks, multiplied by a copy of the synthesized beam, are then iteratively subtracted from the image until no peaks > 4.5 remain; we estimate that 0.03 peaks above this threshold should occur in each set of 8 fields.

Using this technique, we find 30 sources in our 32 fields detected at $> 4.5\,\sigma$ significance. The estimated S_{31} fluxes range from 80 mJy to 2.8 Jy. Correlating these locations with the PMN catalog, we find $S_5 > 100$ mJy counterparts for them all, with probabilities for accidental association $\lesssim 0.01$. Positional errors are typically several arcminutes. However, note that the PMN survey will resolve some of the closest sources, yielding positions which may differ from the effective position as seen by DASI. These factors limit the determination of our absolute pointing error, but we estimate it to be better than $2'$.

Fitting the position of the very brightest sources for each day of data over the observations of a given set of fields shows that pointing drift over $\sim$ 30 days is $< 1'$. Servo tracking jitter is $\ll 1'$ and the fact that point sources appear in the maps with exactly the shape of the synthesized beam confirms this. This last point is demonstrated by the the lower middle and right panels of Figure 5 (see below); this is the field shown in the bottom left panel of Figure 2, which contains the second brightest point source in the A row.

9. RESULTS

Although Fourier plane visibilities are the natural data product of an interferometer, image-plane analysis provides a valuable consistency check on the data quality. Shown in Figure 5 are a subset of the DASI fields, after point source removal and ground subtraction. In these images, point sources identified in the DASI data were removed by subtraction of a delta function model from the visibilities, while ground contamination has been removed by subtraction of a mean visibility, averaged over 8 fields, from each of the 1 hr field integrations. Artifacts of the (u, v) sampling have been reduced in these maps by a variant of the CLEAN algorithm (Högbom 1974), restricted to the −10 dB contour of the primary beam, similar to the procedure described in §8 for finding point sources.

For an interferometer, each visibility is convolved with the autocorrelation of the antenna aperture; in the image plane, this translates into an enveloping of the image by the primary beam. Here the images have been deliberately extended to radii well beyond the central beam area, so that detector noise should dominate near the edges. As can be seen qualitatively in Figure 5, after a simplistic removal of the ground and point source signals, every field shows residual structure in the central region of the beam; as demonstrated in the lower right panel, the rms in radial bins follows the beam profile precisely, tapering to the theoretical noise floor, typically 10 μK (at $\sim 20'$ resolution), far from the beam center.

Images of the same fields observed over different azimuth ranges show repeatable structure, and when images are constructed from visibilities divided into two frequency ranges, the ratio of pixel values is consistent with a thermal spectrum (see Leitch 2000); rigorous, Fourier-plane analogues of these tests are described in Paper II.

We stress that these images are for presentation purposes only; no images are used in our power spectrum analysis, nor are point sources or ground ever subtracted from the visibility data; these foregrounds are modeled in a self-consistent way as part of the constraint matrix formalism presented in Paper II.

The entire complement of 32 DASI fields is shown in Figure 6, after ground and point source removal. Here we show only the central FWHM of each field, corrected for the primary beam taper at the center of the band. Although the S/N is high enough in all these maps that the apparent structure is real, note that the sensitivity is not uniform across the images, but decreases by a factor of 2 at the edges due to the primary beam correction.

10. CONCLUSIONS

We have described the instrumentation, observations and first year data from DASI, a novel interferometric experiment to measure anisotropy in the CMB. During its first season of operation, the instrument functioned superbly, producing 97 days of high quality data on 32 CMB fields, for an average of 24 hours of integration per field, and achieving close to the theoretical noise limits.

With these data, we are able to image ~ 400 square degrees of sky to a typical rms sensitivity of 10 μK (at $\sim 20'$ resolution); we detect structure in the CMB with high S/N in every field. Although the ground has proven to be our largest contaminant, the slowly varying character of this foreground and careful experiment design enables us reliably to recover the CMB component, even in the presence of near-field signals many times the amplitude of the intrinsic fluctuations. As detailed in Paper II and Paper III, these data yield a sensitive new measurement of the CMB power spectrum, providing important constraints on cosmological parameters.

We express our gratitude for the support provided by the Center for Astrophysical Research in Antarctica (CARA), in particular the efforts of Stephan Meyer, Nancy Odalen, Bob Pernic, Dave Pernic, Joe Rottman, and Mark Thoma. We thank Antarctic Support Associates and the 1999–2000 South Pole Station construction crew for extraordinary onsite support, and Eric Chauvin at Vertex/RSI for professional excellence in the design and delivery of the telescope mount. We thank the observatory staff of the Australia Telescope Compact Array, in particular Bob Sault and Ravi Subrahmanyan, for their generosity in providing initial point source observations of the DASI fields. This research is supported by the National Science Foundation under a cooperative agreement (OPP 89-20223) with CARA, a National Science Foundation Science and Technology Center. Support at Caltech is provided by NSF grants AST 94-13935 and AST 98-02989.

REFERENCES

Chamberlin, R. A. & Bally, J. 1995, Int. J. IR and MM Waves, 16, 907
Draine, B. T. & Lazarian, A. 1998, ApJ, 508, 157
Halverson, N. & Carlstrom, J. E. 2001, IEEE-MTT, to be submitted
Halverson, N. W., Leitch, E. M., Pryke, C., et al., 2001, ApJ, submitted, Paper II
Högbom, J. A. 1974, A&AS, 15, 417
Hu, W. & White, M. 1996, ApJ, 471, 30
Jones, M. E. 1997, in Microwave Background Anistropies, proceedings of the XXX1st Recontre de Moriond, 161
King, J. C. & Turner, J. 1997, Antarctic Meteorology and Climatology (Cambridge: Cambridge University Press)
Lay, O. P. & Halverson, N. W. 2000, ApJ, 543, 787
Leitch, E. M., Readhead, A. C. S., Pearson, T. J., et al., 1997, ApJ, 486, L23
Leitch, E. M., et al., 2000, IAU Symposium 201, in press
Padin, S., Cartwright, J. K., Shepherd, M. C., et al., 2000, IEEE Trans. Instrum. Meas., submitted
Pearson, T. J., et al., 2000, IAU Symposium 201, in press, astro-ph/0012212
Pospiezalski, M. W., Lakatosh, W. J., Nguyen, L. D., et al., 1995, IEEE MTT-S Int. Microwave Symp., 1121
Pryke, C., Halverson, N. W., Leitch, E. M., et al., 2001, ApJ, submitted, Paper III
Shepherd, M. C., Pearson, T. J., & Taylor, G. B. 1994, BAAS, 26, 987
Tegmark, M. & Efstathiou, G. 1996, MNRAS, 281, 1297
Tegmark, M., Eisenstein, D. J., Hu, W., et al., 2000, ApJ, 530, 133
White, M., Carlstrom, J. E., Dragovan, M., et al., 1999, ApJ, 514, 12
Wright, A. E., Griffith, M. R., Burke, B. F., et al., 1994, ApJS, 91, 111

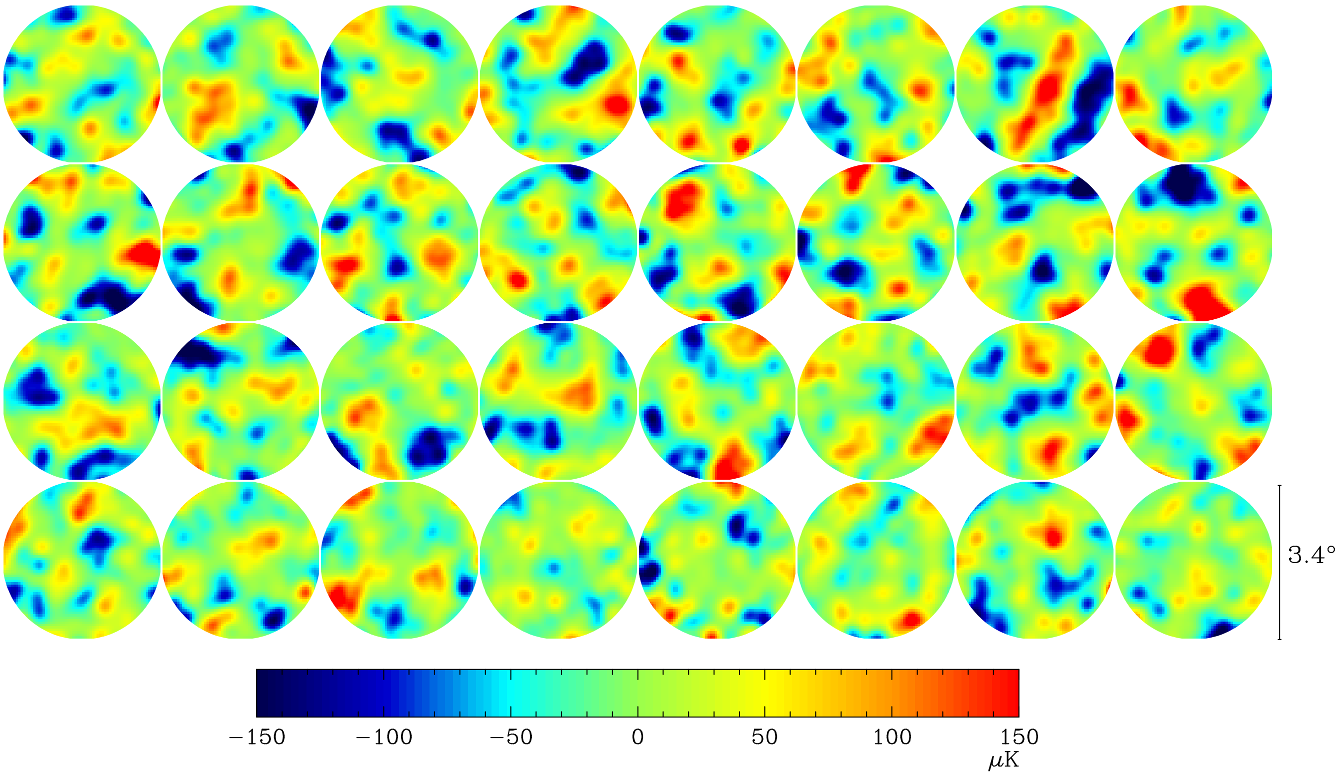

FIG. 6.— Images of the 32 DASI fields, at 20′ resolution. Shown are CLEANed maps of the central 3°.4 FWHM of each primary beam, corrected for the beam taper. Typical rms noise in a 20′ beam is 10 μK at map center. Rows are in order of decreasing elevation: B, A, C, D from top to bottom, with RA increasing to the left.